AN EFFICIENT CATADIOPTRIC SENSOR CALIBRATION BASED ON A LOW-COST TEST-PATTERN

N. Ragot
Institut de Recherche en Systèmes Electroniques EMbarqués
Technopôle du Madrillet - Avenue Galilée - BP 10024, 76801 St Etienne du Rouvray, France

J. Y. Ertaud, X. Savatier, B. Mazari
Institut de Recherche en Systèmes Electroniques EMbarqués
Technopôle du Madrillet - Avenue Galilée - BP 10024, 76801 St Etienne du Rouvray, France

Keywords: Panoramic vision, catadioptric sensor, stereovision, calibration.

Abstract: This article presents an innovative calibration method for a panoramic vision sensor which is dedicated to the three-dimensional reconstruction of an environment with no prior knowledge. We begin this paper by a detailed presentation of the architecture of the sensor. We mention the general features about central catadioptric sensors and we clarify the fixed viewpoint constraint. Next, a large description of the previous panoramic calibration techniques is given. We mention the different postulates which lead us to envisage the method of calibration presented in this paper. A description of the low-cost calibration test pattern is given. The algorithmic approach developed is detailed. We present the results obtained. Finally, the last part is devoted to the result reviewing.

1 INTRODUCTION

Within the framework of applications where the sensor is mobile and where there is no prior knowledge of the environment (no cartographic models available), the knowledge of the exact spatial localization of the sensor is necessary to make a reliable 3D reconstruction. This is known as the paradigm of localization and dynamic environmental modelling (C. Drocourt and Cauchois, 2001). Thus, two kinds of sensors are employed. The first ones are called proprioceptive sensors and are used to provide the mobile with data on its intrinsic state. The second ones are called exteroceptive sensors and are used to provide information to the mobile about the external environment in which it moves. The ignorance of the environmental characteristics impose to the ideal exteroceptive sensor to provide the most complete and precise 3D representation of the environment. This information coupled the proprioceptive sensor data allows a reliable interpretation of the observed environment.
3D exteroceptive perception systems can be classified in different categories (Nitzan 1988). Majority of them are reliable but can not render a wide zone instantaneously. Vision systems and their ability to acquire in a one-shot image all of the information of a volume of a given space has been investigated. This volume, defined by the aperture of the camera, can be increased artificially by combining views given by multiple or rotating cameras (T. Ea and Garda, 2001). Another method consists in coupling a mirror with a camera (S. Baker, 2001), (Zhu, 2001). These are known as catadioptric systems and images obtained are panoramic views of the environment (C. Geyer, 2001).
The architecture of the sensor presented in this paper offers a solution to the problem of 3D perception of an environment with no prior knowledge. This sensor is a panoramic stereovision system constituted of two catadioptric vision sensors. The main objective of this article is to present an innovative calibration which is the preliminary step to the elaboration of a three-dimensional reconstruction. We begin by a detailed presentation of the sensor architecture. We give some general features about catadioptric sensors and we highlight the fixed viewpoint constraint which is presented as the main requirement to process pure perspective images. We refer to calibration techniques for panoramic vision sensors. We detail the proposed calibration principles and we give a large description of the test pattern used. We show the results obtained and we provide a critic analysis about their viability. The last part summarizes the different reflections leaded and gives some work perspectives.

Ragot N., Y. Ertaud J., Savatier X. and Mazari B. (2006).
AN EFFICIENT CATADIOPTRIC SENSOR CALIBRATION BASED ON A LOW-COST TEST-PATTERN.
In *Proceedings of the First International Conference on Computer Vision Theory and Applications*, pages 11-18
DOI: 10.5220/0001374100110018

2 ARCHITECTURE OF THE STEREOVISION PANORAMIC SENSOR

The proposed innovative architecture offers a solution to the problem of 3D perception of an environment with no prior knowledge. The main objective of the study is to develop an exteroceptive stereovision sensor which enables a vision and the most complete 3D reconstruction of the environment. This exteroceptive sensor is made of two catadioptric vision systems.

Each of the catadioptric sensor is composed of a hyperboloid mirror H3S from Neovision coupled with a classic Marlin-F-145C perspective camera from Allied Vision with a 6.5mm focal length. The elements are fixed vertically with their optical axis in common (cf. Figure 1). As a result, the mathematical equations are simplified. Moreover, it enables the simplification of the epipolar relation associating the two omnidirectional sensors. Lastly, it enables the detection of horizontal primitives which is favoured within the framework of our applications.

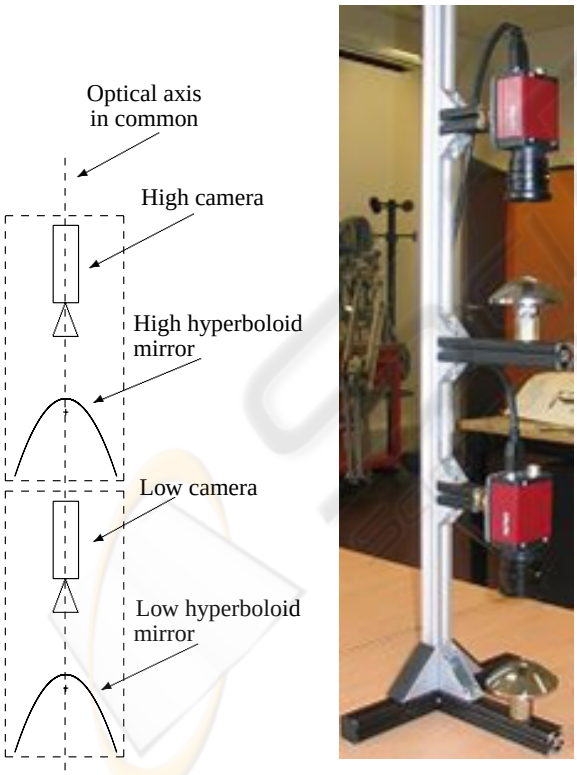

Figure 1: Architecture of the panoramic stereovision sensor. Left: Schema of a cross-section view of the sensor. Right: Image of the sensor developed.

3 CATADIOPTRIC SENSOR: GENERAL FEATURES AND PREVIOUS CALIBRATION WORKS

3.1 General Features

Catadioptric sensors are powerful due to their panoramic vision. Nevertheless, coupling the conventional projective linear model (which enables a pure perspective image formation) to mirror equations can only be done with respect to the fixed viewpoint constraint (Svoboda, 1999). In such a case, the vision system is called a central catadioptric sensor and a geometrically pure perspective image is formed. Two main points have to be mentioned. First, the effective pinhole which is intrinsic to the pinhole model, is also called the principal point of the camera. Second, the effective viewpoint which is intrinsic to the mirror is defined as the focus of the mirror. The fixed viewpoint constraint, also called the single effective viewpoint constraint, is defined as the requirement that vision systems only measure the intensity of light passing through a single 3D point. Work made by Baker et *al.* (S. Baker, 1999) consists in the derivation of the fixed viewpoint constraint equation. They deduce from the obtained results several types of mirrors respecting this constraint (e.g. ellipsoidal, hyperboloidal mirrors). The figure above (cf. Figure 2) illustrates the fixed viewpoint constraint in the case of an hyperboloid mirror. The rays of light coming from a 3D point which seem to meet at the effective viewpoint are reflected by the shape of the mirror and converge at the effective pinhole.

3.2 Previous Calibration Works

The calibration enables to match 3D points in the world frame to 2D pixels in the image planes. Different types of techniques enable to calibrate a catadioptric vision system. The description and classification given below is greatly inspired from the work of El Mouaddib (Mouaddib, 2005).

- The intrinsic calibration consists in the establishment of the intrinsic parameters. In the case of catadioptric sensors, the parameters to be estimated are related to the mirror, lens, CCD matrix and the video acquisition board. This method consists in the exploitation of the mirror imprint on the image and the mirror data dimensions given by the manufacturer. The work made by Fabrizio et *al.* (J. Fabrizio, 2002) is a significant example of this technique. The principle is to exploit the boundaries of the mirror as a calibration pattern. This technique is powerful due to the missing calibration pattern.

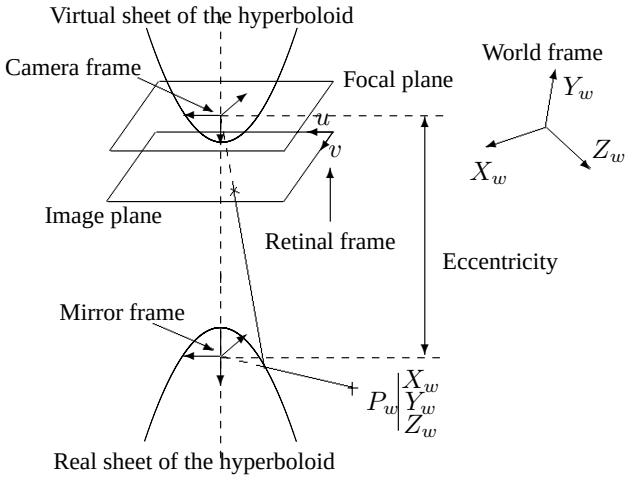

Figure 2: Illustration of the fixed viewpoint constraint in the case of a hyperboloid mirror. The focus of the virtual sheet corresponds to the principal point of the camera (the focus of the camera). The distance between the two foci is called the eccentricity.

Nevertheless it requires the prior knowledge of the geometric mirror characteristics.

- The self-calibration is based on the same principles as for the classical cameras. It consists in the establishment of the fundamental and essential matrices. Thus, it requires a minimum of two image planes and the pixel matching. The pixel matching is based on certain constraints such as uniqueness, ordering, orientation, continuity, disparity gradient. The epipolar constraint is the most powerful one (Faugeras, 1993). We can mention the work of Svoboda et *al.* (T. Svoboda, 1998) which establishes the epipolar geometry for central panoramic cameras using hyperboloid mirrors. The significant works for catadioptric self-calibration are the one made by Kang (Kang, 2000) and Mariottini (G.L. Mariottini, 2005). The first one is based on the derivation of the epipolar relation for catadioptric sensors made of paraboloid mirrors and calibrate the stereovision panoramic system. The second one is a powerful tool developed under MATLAB environment which enables the determination of the epipolar matrices for classical and/or panoramic stereovision sensors.
- The most common method is the one exploiting an external test pattern. This technique is based on the exact knowledge of geometrical figure coordinates (generally points) forming the calibration tool, expressed in a local frame and their 2D matchings. For a sufficient number of matching, an optimization algorithm is applied (e.g. Levenberg-Marquardt (L. Smadja, 2004), (Lacroix et al., 2005)). This method is powerful because it is applicable to all type of catadioptric sensor. Moreover, it enables the estimation of intrinsic and extrinsic parameters. The high number of parameters to be estimated requires a high care for the convergence initialization of the optimization algorithm. One of the significant work is made by Cauchois et *al.* (C. Cauchois and Clerentin, 1999). It exploits a catadioptric sensor formed by a conical mirror. The calibration exploits two type of two plane calibration pattern. One is placed on the top of the cone. The other is perpendicular and enables the estimation of all parameters. The work made by Moldovan (Moldovan, 2004) exploits a cylindrical test pattern formed by a large number of LED which locations are perfectly known. The work made by Ying et *al.* (X. Ying, 2003) is based on the theory of the invariants and exploits the projection of lines and spheres. As well, we can mention the work of Barreto et *al.* (J.P. Barreto, 2005) which demonstrates that three lines are sufficient for the calibration of all central catadioptric sensor.
  As well, this calibration technique is used for applications of active omnidirectional stereovision. We can mention the work made by Marzani et *al.* (F. Marzani and Voon, 2002) which exploits a catadioptric sensor coupled with a laser diode. A bitmap beam is projected on a plane which stands for the external calibration pattern.

4 CALIBRATION PROPOSED

4.1 Postulates

The calibration proposed stems from two postulates:

- The optics (mirrors and lens) are imperfect by nature. Impurities and defaults can not be avoided despite the great precautions taken during the product design (Moldovan, 2004). These imperfections imply local distortions which are difficult to model and thus to take into account.
- The single effective viewpoint constraint is particularly difficult to realize in hardware implementation (Aliaga, 2001).

The calibration exposed intends to establish 3D/2D matchings, the vision sensor being considered as a "black box". This enables to break of the problems listed previously. This calibration method presented can be considered as a generalization of the one developed by Biber et *al.* (P. Biber and Andreas, 2004).

4.2 Method

A catadioptric system provides a circular image of the environment. A pixel, or a sub-pixel p is defined by

its azimut angle α (0<α<360 degrees) and its radius r (cf. Figures 3, 7). α defines the horizontal position of the 3D point $P_M(X_M, Y_M, Z_M)$ and thus is linked to its coordinates X_M, Y_M. In the same way the euclidian distance r defines the vertical position of the 3D point and thus is linked to the coordinate Z_M. Moreover, r can be associated to the angle γ which is defined as the angle from the axis passing through the focus of the mirror and parallel to the axis X_M to the 3D point. The range in which γ lies tightly depends on the mirror geometry. This specification is generally provided by the manufacturer. In our configuration γ lies from -15 to 90 degrees. Finally, γ is linked to the 3D point coordinates and can be expressed as follows (1). The Figure above elaborates the matching between a 3D point to a pixel (cf. Figure 3):

$$\tan\gamma = \frac{Z_M}{X_M} \quad (1)$$

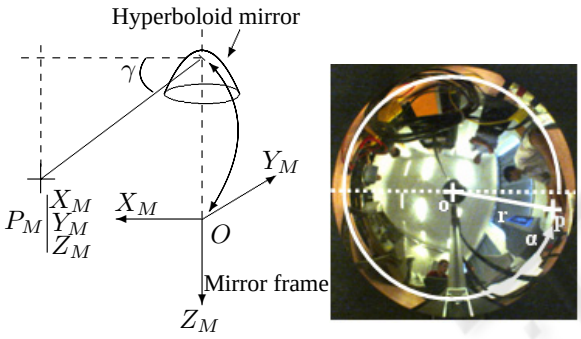

Figure 3: Illustration of the relation linking a 3D point to the pixel radius r. (Right: O stands for image centre, p for pixel position and α for the azimut angle).

Like this, the 3D/2D matching depends on variables α and r. It can be defined as follows:

$$\exists f \ | \ \gamma = f(\alpha, r)$$

4.3 Implementation

The 360 degrees field of view and the 2D spherical coordinates of a pixel or a sub-pixel lead to design and use a cylindrical test pattern. This form is inspired from the works of Moldovan (Moldovan, 2004). The test pattern used is a low-cost one an it is made of rigid PVC. Its height is 1400mm and the internal diameter is 595mm (the thickness of the cylinder is 5mm). This test pattern is formed by a large number of white LED which 3D cartesian coordinates are perfectly known in the frame of the calibration tool. They are vertically arranged with a regular interval. The horizontal angle between each LED is constant (45 degrees). The choice of white color markers is voluntary for two reasons. First, the contrast between the darkness inside the tube and the LED is pronounced. Second, the white light codes the totality of the RGB components which up the sensitivity. Moreover, the angle of diffusion as well as the light intensity are parameters which are particularly be examined. The angle of diffusion is 70 degrees. It is 2.5 times up than for a classical LED. The light intensity is 1190mcd, which is approximately 4 times up than for a common LED. These characteristic enable the obtaining of significant spot lights on each CCD. Next, the sensor is inserted into this test pattern (cf. Figure 4). A particular attention is provided to make sure that the optical axis is aligned with the center of the test pattern.

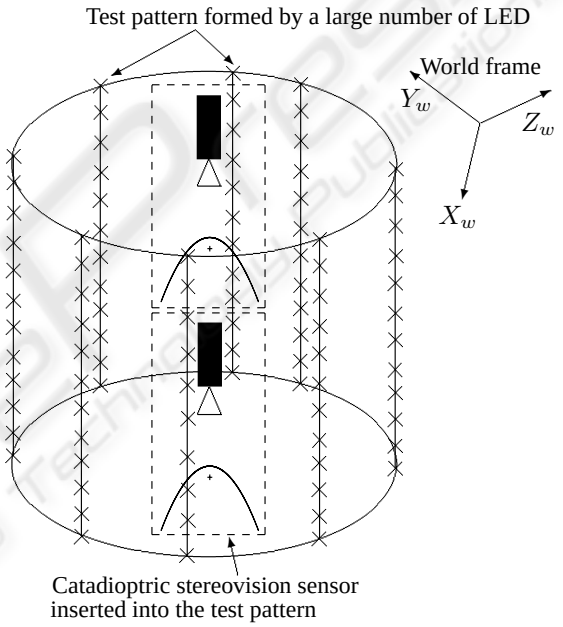

Figure 4: Illustration of the test pattern used to manage the calibration step.

A segmentation algorithm using a local recursion is applied to the two images which enables to reference the markers identified as areas coverage. This local segmentation is done following a criterion of similarity between a reference pixel (p_r) and the pixel in reading (p_i). This criterion is based on the estimation of the color difference by the determination of the euclidean distance. Then, a research of the centre of gravity coordinates is applied to each spot light. This enables to know their exact sub-pixel coordinates. Finally, the 3D points coordinates, the α angle and the euclidean distance r being known, the function $\gamma = f(\alpha, r)$ can be established (cf. Figure 5).

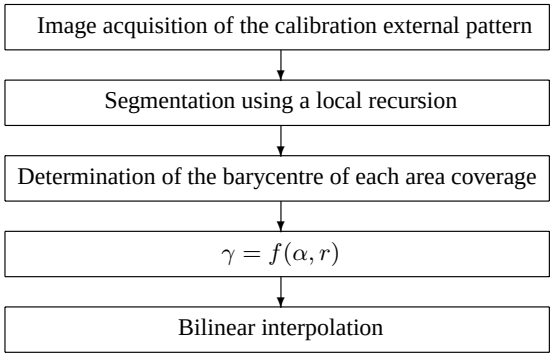

Figure 5: The block diagram describing the calibration process.

5 RESULTS

The markers are referenced in a cartesian frame $(O, X_{TP}, Y_{TP}, Z_{TP})$, which is located at the bottom centre of the cylinder (cf. Figure 6). They are expressed in cylindrical coordinates and are summarized in the table (cf. Table 1). The positioning of the markers implies that for each LED Bar Bi, the parameter h_i defined as the vertical component, is the single one variable.

The particular configuration, in which Z_{TP} axis is merged with the optical axis of the sensor, enables an immediate expression of the coordinates of the markers in each mirror frame. Thus, the angle γ which is linked to the position of the markers and expressed in each mirror frame can be easily determined. Moreover, for points located at a same altitude, the angle γ is equivalent.

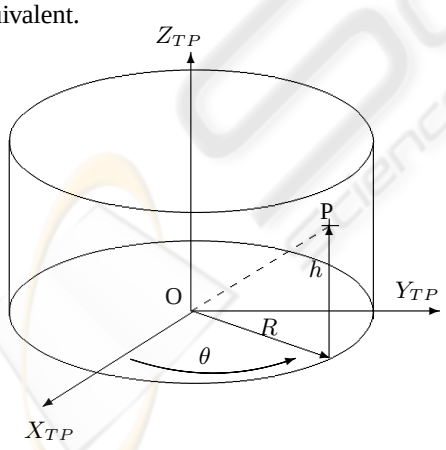

Figure 6: Localisation of the frame of the test-pattern.

The image acquisitions are carried out so that the eight markers located at a same altitude, are lighted simultaneously (cf. Figure 7). As mentioned previously, simple image processings permit the determination of homogenous regions and all markers barycentre localisation. Thus, the determination of pixel or sub-pixel polar coordinates (r,α) are obtained. These two parameters are expressed in a local image frame (O', u', v') which the point O' is located at the centre of the images and the axes (u', v') are parallel to those of the retinal plane (u, v). The results are summarized on the four next tables. The tables above (cf. Tables 2, 3) describe the results obtained for the low sensor and the next ones (cf. Tables 4, 5) those obtained for the high sensor (for the tables 2 to 5, the radius is in pixel unity, the angle α is in degree). The figures (cf. Figure 8, 9) illustrate the the functions $\gamma = f(\alpha, r)$ obtained for the two sensors constituting the panoramic stereovision sensor.

Table 1: Cylindrical coordinates of the markers. Bi stands for LED Bar. Considering each LED bar separately, h_i is the only variable parameter following the vertical axis (Z_{TP}).

	B1	B2	B3	B4	B5	B6	B7	B8
Radius R (mm)	289.5	289.5	289.5	289.5	289.5	289.5	289.5	289.5
θ (degrees)	0	45	90	135	180	225	270	315
h_1	50	50	50	50	50	50	50	50
h_2	150	150	150	150	150	150	150	150
h_3	250	250	250	250	250	250	250	250
h_4	350	350	350	350	350	350	350	350
h_5	450	450	450	450	450	450	450	450
h_6	550	550	550	550	550	550	550	550
h_7	650	650	650	650	650	650	650	650
h_8	750	750	750	750	750	750	750	750
h_9	850	850	850	850	850	850	850	850
h_{10}	950	950	950	950	950	950	950	950
h_{11}	1050	1050	1050	1050	1050	1050	1050	1050
h_{12}	1150	1150	1150	1150	1150	1150	1150	1150
h_{13}	1250	1250	1250	1250	1250	1250	1250	1250
h_{14}	1350	1350	1350	1350	1350	1350	1350	1350

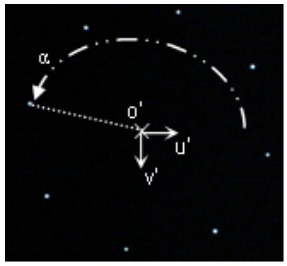

Figure 7: Illustration of an image obtained during the calibration step. The local image frame and the azimut angle α are mentioned. α is defined as the angle from u' to the 2D point considered.

Table 2: Low sensor calibration data. The four first LED bars Bi_L.

$B1_L$		$B2_L$		$B3_L$		$B4_L$	
radius	α	radius	α	radius	α	radius	α
370.96	33.17	371.74	78.28	366.44	122.80	366.28	168.66
260.94	33.49	261.46	77.23	257.22	122.88	259.10	168.87
191.43	33.62	190.12	78.03	185.00	123.09	186.96	168.89
147.67	32.80	145.78	76.92	142.21	122.45	141.79	168.61
116.81	32.05	115.54	75.77	113.42	123.11	113.09	168.78
96.39	32.64	94.50	76.77	92.56	123.71	91.88	169.33
81.03	31.21	79.67	75.11	77.42	122.91	77.02	168.77
69.95	31.93	67.65	73.89	66.17	123.79	66.28	168.69
60.68	31.82	58.95	75.21	57.65	125.39	57.02	169.90
53.67	30.19	51.53	75.96	50.93	124.45	50.10	169.65
47.90	30.06	46.02	72.93	44.91	122.20	44.66	168.37

Table 3: Low sensor calibration data. The four last LED bars Bi_L.

$B5_L$		$B6_L$		$B7_L$		$B8_L$	
radius	α	radius	α	radius	α	radius	α
367.38	213.91	364.42	259.22	369.42	304.89	375.05	349.70
256.71	213.58	259.43	259.38	261.23	305.37	263.51	349.94
186.34	214.66	188.20	259.40	189.89	305.28	191.15	349.75
142.42	214.66	144.23	259.90	145.87	304.65	146.91	349.80
113.46	213.72	115.05	259.15	116.19	304.28	116.27	349.59
93.64	213.73	95.13	257.85	95.60	305.32	95.84	349.78
77.43	213.73	79.17	260.10	80.81	305.24	81.01	350.04
66.20	213.97	67.86	256.52	69.36	306.15	70.11	350.14
57.87	214.76	59.16	258.62	60.21	305.53	61.04	349.61
50.59	214.96	51.70	260.53	53.63	306.70	54.22	349.37
45.26	215.05	46.42	255.76	47.74	307.26	49.07	349.43

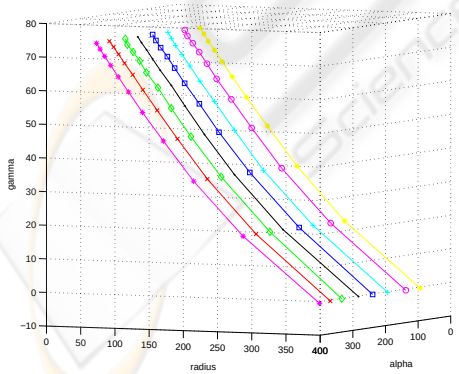

Figure 8: Illustration of the function $\gamma = f(\alpha, r)$ obtained for the low sensor.

Table 4: High sensor calibration data. The four first LED bars Bi_H.

$B1_H$		$B2_H$		$B3_H$		$B4_H$	
radius	α	radius	α	radius	α	radius	α
460.37	32.89	461.61	77.69	461.45	122.77	458.85	167.92
371.57	32.38	380.46	77.19	386.66	121.97	398.91	167.84
262.05	32.29	267.33	77.50	269.95	122.76	275.66	167.64
192.46	33.06	194.41	77.76	194.35	122.45	196.32	167.34
146.95	32.51	148.70	75.55	148.37	121.13	148.38	167.15
119.07	33.08	119.80	75.51	119.17	122.06	118.37	166.81
98.84	33.80	99.83	76.31	99.08	122.02	97.36	166.33
84.30	33.06	85.68	75.61	84.65	121.73	82.62	165.99
72.93	32.32	74.46	75.21	73.25	120.67	71.55	166.25
64.08	33.10	65.42	74.36	64.86	120.30	63.06	165.30
56.91	34.21	58.49	73.21	58.00	120.45	56.14	165.56
51.83	35.36	52.66	75.56	52.04	122.27	50.68	165.13

Table 5: High sensor calibration data. The four last LED bars Bi_H.

$B5_H$		$B6_H$		$B7_H$		$B8_H$	
radius	α	radius	α	radius	α	radius	α
456.26	213.07	454.36	258.34	454.99	302.67	457.48	348.01
393.00	212.64	388.01	257.62	376.95	301.90	370.19	348.15
273.74	211.98	268.91	256.98	262.48	302.24	260.10	348.01
196.09	211.68	193.45	256.36	190.56	302.90	189.86	348.76
145.99	211.37	145.36	255.92	143.81	303.44	144.52	349.23
115.96	211.15	114.59	255.60	114.39	303.85	116.84	349.64
96.13	210.64	94.34	257.20	94.82	304.65	96.37	349.84
81.24	210.30	79.66	255.13	80.15	304.56	81.93	350.16
70.22	210.83	68.82	256.76	69.17	304.51	71.24	351.11
61.22	210.41	60.26	254.22	60.71	304.56	62.18	350.74
54.49	209.69	53.03	254.05	53.45	306.43	55.35	351.69
49.05	209.29	47.41	255.98	47.88	307.48	49.81	351.92

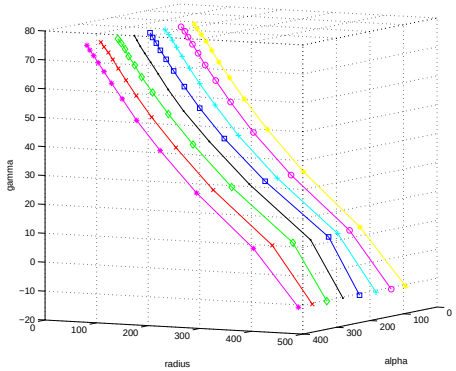

Figure 9: Illustration of the function $\gamma = f(\alpha, r)$ obtained for the high sensor.

6 DISCUSSION

From the results presented, two main points can be discussed.
The markers positioned onto a same vertical bar must have, theoretically, similar angle α values either for the low sensor or the high sensor. Considering the low sensor, the mean deviation fluctuates from 0.183 to 1.306 (cf. Table 6) (all the quantities enumerated in this paragraph are in pixel unity). In the case of the high sensor, the mean deviation varies from 0.643 to 1.137 (cf. Table 7). The difference of the mean α values of the low and high sensors gives information about the alignment of the sensors on a common optical axis. This difference varies from 0.029 to 3.119 (cf. Table 8). The vertical alignment of the sensors is one of the main requirement for the development of stereovision sensors. This parameter has an effect on two notions. The first one deals with the self-calibration and more precisely the establishment of the fundamental and essential matrices. Thus, a too important error may affect significantly the pixel matchings. The second one is linked to the resolution of the sensor. A misalignment of the two sensors implying an error of 3.119 may be sufficient for applications which do not require a high resolution, and probably not for fine applications.

From the different experiences conducted, it is difficult to realize a perfect alignment in hardware implementation. An alignment correction by an analytical procedure is envisaged to break of this problem.

Table 6: Mean deviation of the parameter α in the case of the low sensor.

Low Sensor	
	Mean deviation of α
$B1_L$	0.959
$B2_L$	1.306
$B3_L$	0.720
$B4_L$	0.366
$B5_L$	0.520
$B6_L$	1.148
$B7_L$	0.651
$B8_L$	0.183

Table 7: Mean deviation of the parameter α in the case of the high sensor.

High Sensor	
	Mean deviation of α
$B1_H$	0.643
$B2_H$	1.112
$B3_H$	0.718
$B4_H$	0.845
$B5_H$	0.894
$B6_H$	1.043
$B7_H$	1.267
$B8_H$	1.137

A similar analysis can be developed in the case of the radius parameter r. The markers located at a same altitude must have, theoretically, equal radius values. For the low sensor the mean deviation fluctuates from 1.201 to 2.833 (cf. Table 9). In the case of the high sensor this deviation fluctuates from 1.590 to 2.399 (cf. Table 10). The value 8.427 is not taken into account because it is not a relevant value towards the homogeneousness of the values obtained. This evaluation is linked to the alignment between the vertical axis of the frame of the test-pattern (Z_{TP}) and the optical axis of the panoramic stereovision sensor. In hardware implementation, it is difficult to merge the two axes. An analytical procedure is envisaged to break of this problem.

Table 8: Evaluation of the difference of the mean values α. Highlighting of the difficulty to get a common optical axis for the two sensors.

	Difference of the mean value of the parameter α
$B1_L/B1_H$	1.083
$B2_L/B2_H$	0.055
$B3_L/B3_H$	1.629
$B4_L/B4_H$	2.351
$B5_L/B5_H$	3.119
$B6_L/B6_H$	2.587
$B7_L/B7_H$	1.417
$B8_L/B8_H$	0.029

Table 9: Mean deviation of the parameter r in the case of the low sensor.

Low Sensor	
	Mean radius
h_1	2.833
h_2	1.834
h_3	2.009
h_4	1.948
h_5	1.240
h_6	1.312
h_7	1.434
h_8	1.392
h_9	1.201
h_{10}	1.345
h_{11}	1.434

Table 10: Mean deviation of the parameter r in the case of the high sensor.

High Sensor	
	Mean radius
h_3	2.399
h_4	8.427
h_5	4.537
h_6	1.858
h_7	1.590
h_8	1.830
h_9	1.682
h_{10}	1.786
h_{11}	1.590
h_{12}	1.628
h_{13}	1.652
h_{14}	1.631

7 CONCLUSION

The main objective of this article is to present an innovative calibration method applied to a panoramic stereovision sensor. The sensor presented is made of two catadioptric sensors coupled vertically with their optical axis in common. The calibration technique is based on the characteristics of the images obtained by a catadioptric sensor. A pixel or sub-pixel can be expressed in polar coordinates (α, r) and the radius r is linked to the coordinates of the point expressed in the 3D frame. Thus, we use a low-cost cylindrical test-pattern made of several markers which cylindrical coordinates are known. Classical image algorithms are applied to determine the polar

coordinates of the pixel or sub-pixel matching. The function linking the 3D points to the 2D points is obtained and a local bilinear interpolation is carried out to get the 3D/2D matchings for points which 3D coordinates are known.

Three main perspectives of work are envisaged.

- The first one consists in developing analytical procedures which enable the correction of the misalignment of the two sensors and the misalignment between the optical axis and the vertical axis of the frame of the test-pattern.
- The second one is linked to the development of an analytical calibration method which is based on the minimization of a criterion function. This function is defined as the non-linear equation linking a 3D point considered in the environment and a 2D point on the image plane (Svoboda, 1999). We propose to use the Levenberg-Marquardt algorithm which is a classical optimization technique for non-linear equation.
- The third one deals with the self-calibration of the panoramic stereovision sensor. It consists in the establishment of the fundamental and essential matrices. This calibration method is linked to the epipolar geometry which enables the matchings of pixels in different image planes. This geometry is well known for classical vision systems and has been recently established for catadioptric sensors (Svoboda, 1999).

REFERENCES

Aliaga, D. (2001). Accurate catadioptric calibration for real-time pose estimation inroom-size environments. In *8th IEEE International Conference on Computer Vision*, volume 1, pages 127–134.

C. Cauchois, E. Brassart, C. P. and Clerentin, A. (1999). Technique for calibrating an omnidirectional sensor. In *International Conference on Intelligent Robots and Systems*.

C. Drocourt, L. Delahoche, E. B. and Cauchois, C. (2001). Simultaneous localization and map building paradigm based on omnidirectional stereoscopic vision. In *Proceeding IEEE Workshop on Omnidirectional Vision Applied to Robotic Orientation and Nondestructive Testing*, pages 73–79.

C. Geyer, K. D. (2001). Catadioptric projective geometry. *International Journal of Computer Vision*, 43:223–243.

F. Marzani, Y. Voisin, A. D. and Voon, L. F. L. Y. (2002). Calibration of a 3d reconstruction system using a structured light source. *Journal of Optical Engineering*, 41:484–492.

Faugeras, O. (1993). *Three-dimensional computer vision : a geometric viewpoint*. MIT Press, Cambridge, Massachusetts, 4th edition.

G.L. Mariottini, D. P. (2005). The epipolar geometry toolbox : multiple view geometry for visual servoing for matlab. *IEEE Robotics and Automation Magazine*.

J. Fabrizio, J.-P. Tarel, R. B. (2002). Calibration of panoramic catadioptric sensors made easier. In *Workshop on Omnidirectional Vision*.

J.P. Barreto, H. A. (2005). Geometric properties of central catadioptric line images and their application in calibration. *IEEE Transactions on Pattern Analysis and Machine Intelligence*, 27:1327–1333.

Kang, S. (2000). Catadioptric self-calibration. In *International Conference on Computer Vision and Pattern Recognition*, volume 1, pages 201–207.

L. Smadja, R. Benosman, J. D. (2004). Cylindrical sensor calibration using lines. In *5th Workshop on Omnidirectional Vision, Camera Networks and Non-Classical Cameras*, pages 139–150.

Lacroix, S., Gonzalez, J., El Mouaddib, M., Vasseur, P., Labbani, O., Benosman, R., Devars, J., and Fabrizio, J. (2005). Vision omnidirectionnelle et robotique. rapport final. Technical report, LAAS, CREA, LISIF.

Moldovan, D. (2004). A geometrically calibrated pinhole model for single viewpoint omnidirectional imaging systems. In *British Machine Vision Conference*.

Mouaddib, M. E. (2005). La vision omnidirectionnelle. In *Journée Nationale de la Recherche en Robotique*.

P. Biber, H. Andreasson, T. D. and Andreas, A. S. (2004). 3d modeling of indoor environments by a mobile robot with a laser scanner and panoramic camera. In *IEEE/RSJ International Conference on Intelligent Robots and Systems*.

S. Baker, S. N. (1999). A theory of single-viewpoint catadioptric image formation. *International Journal of Computer Vision*, 35:175–196.

S. Baker, S. N. (2001). *Panoramic Vision: Sensors, Theory and Applications*, chapter Single viewpoint catadioptric cameras, pages 39–73. Springer-Verlag, 1st edition.

Svoboda, T. (1999). *Central panoramic cameras. Design, geometry, egomotion*. PhD thesis, Czech Technical Univeristy.

T. Ea, O. Romain, C. G. and Garda, P. (2001). Un capteur de sphéréo-vision stéréoscopique couleur. In *Congrès francophone de vision par ordinateur ORASIS*.

T. Svoboda, T. Pajdla, V. H. (1998). Epipolar geometry for panoramic cameras. In *5th European Conference on Computer Vision*, volume 1406, pages 218–232.

X. Ying, Z. H. (2003). Catadioptric camera calibration using geometric invariants. In *International Conference on Computer Vision*, pages 1351–1358.

Zhu, Z. (2001). Omnidirectional stereo vision. In *10th IEEE ICAR Workshop on Omnidirectional Vision*.